Time stretching of the GeV emission of GRBs: Fermi LAT data vs geometrical model

Maxim S. Piskunov[1,2*] and Grigory I. Rubtsov[2,3†]

[1]Faculty of Physics, Moscow State University, Moscow, Russia

[2]Institute for Nuclear Research of the RAS, Moscow, Russia

[3]Novosibirsk State University, Novosibirsk, Russia

November 3, 2014

Abstract

It is known that the high energy ($> 100\,\mathrm{MeV}$) emission of gamma-ray bursts is delayed with respect to the low energy emission. However, the dependence of light curves on energy has not been studied for the high energy bands. In this paper we consider the bursts observed by Fermi-LAT from 2008 August 4 to 2011 August 1, for which at least 10 photons were observed with energy greater than 1 GeV. These include 4 bursts: GRB 080916C, GRB 090510, GRB 090902B, and GRB 090926A. We use the Kolmogorov-Smirnov test to compare the light curves in the two bands, $100\,\mathrm{MeV} < E < 1\,\mathrm{GeV}$ and $1\,\mathrm{GeV} < E < 300\,\mathrm{GeV}$. For GRB 080916C and GRB 090510 the light curves in two bands are statistically compatible. However, for GRB 090926A, the higher-energy light curve is stretched compared to the lower-energy one with a statistical significance of 3.3σ and, for GRB 090902B, on the contrary, the lower-energy curve is stretched with 2.3σ significance. We argue that the observed diversity of stretching factors may be explained in a simple geometrical model. The model assumes that the jet opening angle depends on the emission energy in a way that the most energetic photons are radiated near the axis of the jet. All the bursts are considered equivalent in their rest frames and the observed light curves differ only due to different redshifts and view directions. The model conforms to the total burst energy constraint and matches the Fermi LAT observations of the fraction of GRBs visible in $100\,\mathrm{MeV} < E < 1\,\mathrm{GeV}$ band, which may be observed at higher energies. The model predicts the distribution of observable stretching factors, which may be tested in the future data. Finally, we propose a way to estimate observer's off-axis angle based on stretching factor and fraction of the high-energy photons. The code for modeling is open source and is publicly available on GitHub (`https://github.com/maxitg/GammaRays`).

1 Introduction

Gamma-ray bursts (GRBs) are among the most energetic events in the Universe. Therefore, the studies of the emission mechanism and phenomenology of GRBs may provide the new knowledge in particle physics. Moreover, the GRBs are observed from cosmological distances and therefore bear an imprint of the late-time evolution of the Universe. An extensive studies of these explosions led to a number of interesting results, see [1, 2] for a review. In particular, the total energy emitted in gamma-rays during a burst was found to be similar for the different GRBs within an order of magnitude [3]. This indicates that the most of the bursts have similar energetics in their rest frames. Several observations are related to the temporal variations of spectra. This way, the spectral lags were found between different low energy bands [4] and the very-high-energy radiation was discovered to be extended relative to the x-ray emission [5, 6, 1].

*maxit@ms2.inr.ac.ru

†grisha@ms2.inr.ac.ru

We decided to elaborate on that result, and, using the data from Large Area Telescope (LAT) of Fermi satellite [7], explore the spectral variations between different high energy bands, specifically $(100\,\mathrm{MeV}, 1\,\mathrm{GeV})$ and $(1\,\mathrm{GeV}, 300\,\mathrm{GeV})$ (we call them low and high energy bands throughout the paper). In particular, we use the Kolmogorov-Smirnov test to compute the time stretching of radiation in one of these bands compared to the other.

We take the GRB list from the Fermi-LAT catalog [8]. Tables 2 and 4 in [8] provide the time, durations and locations of the bursts, which we use to download observational data from the LAT Data Server[1]. We also download events during a day before the burst, and use the technique introduced in [9] to estimate background radiation in both energy bands.

Most of the bursts in the catalog, however, do not have enough events with over 1 GeV energies to do desired computations, so we choose only those bursts, from which at least 10 photons were detected in the high energy band. It leaves 4 of them: GRB 080916C [10], GRB 090510 [11], GRB 090902B [12] and GRB 090926A [13].

For these 4 bursts we compute both high and low energy distributions of photon arrival times, and subtract background estimates from them. This makes CDFs non-monotonous and, rigorously speaking, we cannot use the 2-sample Kolmogorov-Smirnov test on it. However, since the number of photons is much higher than estimated background, this non-monotonicity is negligible, and will not harm KS-test results much.

Finally, we stretch the high energy CDF by different factors, and compare it to the low energy CDF using the KS-test. If we require 2σ-significant probability to exclude a particular stretching factor, then the stretching factor of 1 (which means no stretching) is allowed for GRB 080916C and GRB 090510. For the other two bursts the stretching factor of 1 is, however, excluded. For GRB 090902B it should be smaller than 1, so the low energy light curve is stretched with respect to the high energy one (see fig. 5). And for GRB 090926A even more significant deviation from the stretching factor of 1 is observed in the opposite direction. The high energy light curve of GRB 090926A is stretched with respect to the low energy one by a factor of at least 1.99 (see fig. 6). All observed stretching factors are summarized in table 2, and the detailed procedure for computing them is described in section 2 of the paper.

We propose that this result can be explained by the curvature effects (that is the effects of the jet geometry). These effects were explored by multiple authors [14, 15, 16]. However, these studies were only concerned with x-ray radiation, and, even more importantly, they assumed that the distribution of radiation sources is homogeneous throughout the jet. We propose a contrary idea: that the highest energy radiators are concentrated near the axis of the jet, so that the jet opening angle depends on energy. We cannot prove this assumption rigorously, but we have arguments supporting it.

First of all, there are around 750 GRBs detected by GBM, half of which were in the LAT field of view at the moment of observation [1]. However, only about 30 of them were detected by the LAT, and only 4 of them were bright in the high energy band. If we extrapolate the uniform jet model to very high energies, this observation would mean that these groups of bursts are internally different: some of them produce VHE radiation, while others do not. These differences are hard to explain given that burst energetics are similar [3]. Nevertheless, these differences in burst counts can easily be explained by our model. In our model, the opening angle of a jet is inversely proportional to the energy of photons it radiates. Therefore the most common scenario is that the off-axis angle of an observer is smaller than the low energy jet opening angle, but much larger than the opening angle of a high energy jet. Because of that, most of the bursts can only be seen at low energies. The 4 bursts we study in this paper were seen, according to our model, from the lowest off-axis angles.

Second, consider the plasma right after its ejection from the central engine. Two processes happen there simultaneously:

1. Particles near the jet boundary collide and change their movement directions, therefore increasing the opening angle of the jet.

2. Particles lose energy, therefore decreasing radiation frequency emitted by the jet.

[1] `http://fermi.gsfc.nasa.gov/cgi-bin/ssc/LAT/LATDataQuery.cgi`

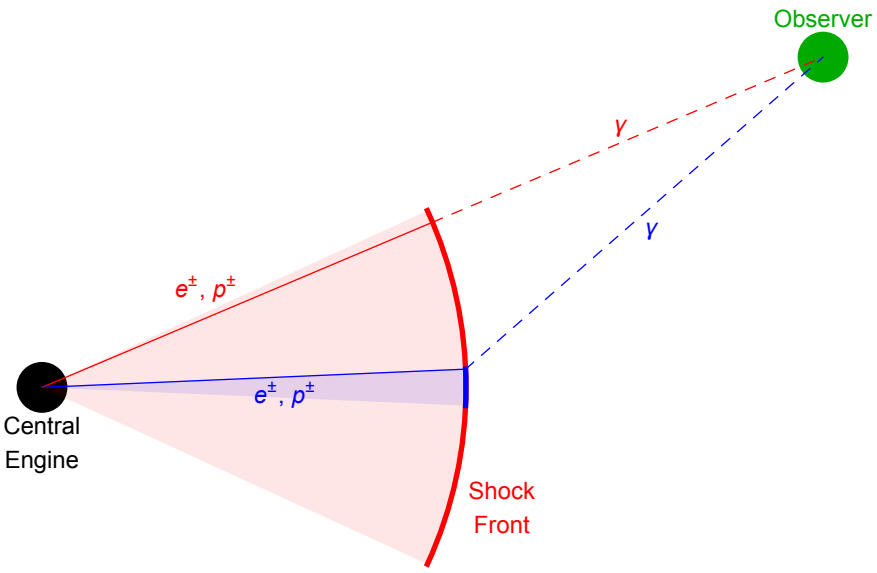

Figure 1: Model Overview. Here red and blue cones represent the regions through which low and high energy plasma propagates. In case depicted the observer's off-axis angle is smaller than the opening angle of the low energy jet, so, due to the relativistic beaming effect, the most of the observable low energy photons will travel along the straight line from the central engine. Also, the observer's off-axis angle is larger that the opening angle of the high energy jet, so the high energy radiation will still originate near the center of the jet (because it is the only place where there are high energy radiators). The observation time of a photon is a sum of two things: the time interval spent in plasma as a radiator (which approximately equals to the distance from the central engine to the point of emission); and the time interval from emission to detection (which is the distance from the point of emission to the observer's location). Given a position of the shock front, this sum is larger for high energy photons. Because of that, high energy emission will be observed later throughout the burst duration, therefore the high energy light curve will be stretched.

We argue that these two processes are correlated, for they happen due to the same particle interaction processes. And since they are correlated, jets with larger opening angles should have lower energies, which is the assumption we are trying to justify.

Finally, our assumption is able to explain the non-trivial stretching factor of both GRB 090902B and GRB 090926A. Detailed computations are described in section 3, but you can see the main idea on figure 1. Computations confirm that this qualitative picture is indeed correct. You can see a sample light curves on figure 2, and predicted distribution of stretching factors on figure 7.

Results of our study, including a few predictions of our model and a new method for estimating jet observation angles, are summarized in section 4, and the caveats are discussed in section 5.

2 Observations

2.1 Fermi LAT Photon Selection

Before we start to compute the Kolmogorov-Smirnov probabilities, we need to download the actual observational data from the Fermi LAT data server. We take the data about the bursts from the catalog [8], which contains all the bright bursts seen by the LAT since 2008 August 4 to 2011 August 1. Specifically, we take 4 pieces of information from the tables 2 and 4 there:

- GBM trigger time (table 2). It is used as a reference point for the GRB time.

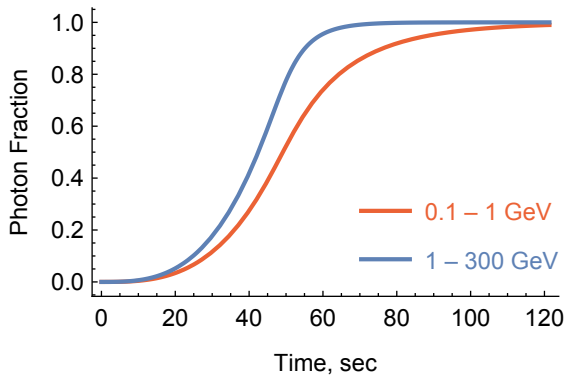

(a) Stretching factor $\kappa = 0.819$, redshift $z = 1.82$, off-axis angle $\chi = 0$.

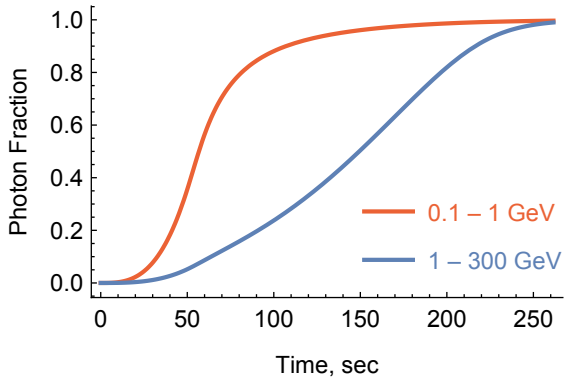

(b) Stretching factor $\kappa = 2.43$, redshift $z = 2.106$, off-axis angle $\chi = 5.90 \times 10^{-3}$.

Figure 2: High and low energy light curves produced by the geometrical model. Burst parameter values are the same as discussed in section 4.1.

GRB Name `name`	GBM Trigger Time MET, sec `time`	R.A. J2000, deg `location.ra`	Dec. J2000, deg `location.dec`	Location Error deg `location.err`	T_{05} sec `startOffset`	T_{95} sec `endOffset`
080825C	241 366 429.105	233.9	−4.5	0.75	3.2	29.4
080916C	243 216 766.614	119.85	−56.64	0.0001	5.0	209.8
081006	244 996 175.173	136.32	−62.05	0.52	0.7	115.0
081024B	246 576 161.864	322.95	21.2	0.22	0.1	191.0
090217	256 539 404.560	204.83	−8.42	0.35	6.2	68.0
090323	259 459 364.630	190.71	17.053	0.0001	15.9	293.9
090328	259 925 808.510	90.67	−41.715	0.0002	18.8	652.9
090510	263 607 781.971	333.55	−26.583	0.0004	0.6	45.6
090626	267 683 530.880	170.03	−33.49	0.22	52.2	299.9
090902B	273 582 310.313	264.94	27.324	0.001	7.7	825.0
090926A	275 631 628.990	353.4	−66.32	0.01	5.5	225.0
091003	276 237 347.585	251.52	36.625	0.0005	3.9	452.6
091031	278 683 230.850	71.49	−57.65	0.23	3.1	206.2
100116A	285 370 262.240	305.01	14.43	0.17	3.0	141.0
100414A	292 904 423.990	192.11	8.693	0.0005	17.4	288.6
110120A	317 231 981.230	61.5	−12.0	0.36	0.5	112.8
110428A	325 675 112.410	5.59	64.849	0.000 01	10.7	407.6
110721A	332 916 465.760	333.2	−38.5	0.20	0.1	239.0
110731A	333 803 371.954	280.504	−28.537	0.0001	3.0	24.1

Table 1: Burst data used in our study. The third row contains the corresponding `GRBurst` class variable names. The data is taken from the tables 2 and 4 of [8]. `https://github.com/maxitg/GammaRays/blob/master/GRObservations/bursts`

- Location of the GRB (table 2). We need burst locations to filter out photons coming from other sources.
- Location error (table 2). Location errors are used to improve accuracy of filtering, specifically to avoid losing statistics by filtering too much.
- T_{05} – T_{95} interval of the LAT-detected emission (table 4). We need precise intervals for two things. First, to understand where is the fixed point of the stretching (T_{05} is used as a proxy for that). Second, the burst interval is used to download events data from the data server.

The data obtained is summarized in table 1.

To have a decent safety margin, we download the data about observed photons extended in time by 50% to both past and future relative to the table 1. For background estimation, we also download observational data during a day before the burst. Exact values we put into the web form are listed in appendix A.

Before reading the data, we need to apply the basic filtering as described in Fermi guidelines[2] (the actual code, and all parameters values we use to invoke Fermi Science tools are listed in appendix A). Two tools from the Fermi Science Tools package[3] are used for that task (the same filtering is applied to both burst and background data).

First, we use `gtselect`. We filter the Earth limb emission with it below the zenith angle of 100°. We also filter out photons with transient event class for a reason described in the next section.

The second one we use is `gtmktime`. It uses the spacecraft file as well as events file, and filters out time periods when Fermi LAT was not operational. Running `gtmktime` is also required for exposure maps calculation, which we'll need later on.

Now, with basic filtering done, we can read events data from `timed.fits`. This file, however, contains observations of a large area of the sky. Before using the data obtained from it, we should perform a more elaborate filtering by location using the point spread function of Fermi LAT, which can be computed with `gtpsf` tool. We use 300 energy bins from 100 MeV to 300 GeV, and 300 angular bins with maximal angle being 30°. We use `gtltcube` tool to compute livetime maps, which are `gtpsf` need. Note, that we need PSFs for all Instrument Response Functions of Fermi, that is for all event classes (transient, source, clean and ultraclean) and conversion types (back and front).

To understand how to use obtained PSFs, imagine a stream of photons coming from some source located at some coordinates θ, ϕ. Ideally, all the coordinates measured for the photons coming from the source should be the same. However, due to measurement errors, they would be spread across some region of the sky. If we find the region such that, say, 95% of photons coming from the source are measured inside of it, we can filter out all the other photons without losing too much statistics, and significantly reducing background. `gtpsf` approximates these regions as circles, and the files generated in the previous step contain the observation probability densities as functions of distance from the source and photon energies. We, however, need an integral quantity, that is given the radius, we want to know the fraction of photons observed inside the circle of this radius. We can compute this fraction by summing over the probability densities:

$$\begin{aligned} p(n) &= \int_0^n \texttt{pdf[i]}\, 2\pi \sin(\texttt{angles[i]})\, \mathrm{d}i \\ &\approx \sum_{i=0}^{n} \frac{\texttt{pdf[i]} + \texttt{pdf[i+1]}}{2} 2\pi \left(\cos(\texttt{angles[i]}) - \cos(\texttt{angles[i+1]})\right) \end{aligned}$$

Here `pdf[i]` is the probability density in the point separated from the source by an angle `angles[i]`. And $p(n)$ is the probability to observe a photon closer to the source than `angles[n]`. We find probabilities for intermediate angles by linear interpolation. Finally, we can compute the inverse value $\theta_{\text{spread}}(p)$ (that is a distance as a function of probability) by binary search. Note, that $\theta_{\text{spread}}(p)$ depends on the photon energy, event class, and conversion type. We should use the appropriate function for each photon. The spread angles for intermediate energies are linearly interpolated.

[2] `http://fermi.gsfc.nasa.gov/ssc/data/analysis/scitools/data_preparation.html`

[3] `http://fermi.gsfc.nasa.gov/ssc/data/analysis/scitools/overview.html`

Finally, to finish the filtering, we filter out all the photons, for which their location is separated from the source by more that $\theta_{\text{spread}}(0.95) + \texttt{location.err}$, where `location.err` is the uncertainty in the burst location (see table 1).

Now we have a decent set of photons, which we can use for analysis. However, some of the photons in this set are still originated from background, and not from the source. We cannot filter out these photons, but we can substitute a linear component of background estimating it from a long time period before the burst. In order to perform this computation, we need an exposure map, which will be discussed in the following section.

2.2 Exposure Maps and Background Estimation

The exposure map can be computed with the `gtexpcube2` tool. We compute it with 300 energy bins from 100 MeV to 300 GeV.

The generated `expcube` files contain exposures as functions of energy and location on the sky. We use trilinear interpolation to compute exposures for all energies and locations.

Knowing the exposures, we can now use the method introduced in the appendix of [9] to estimate the linear component of background from the data observed before the burst. We compute two background estimates: for low and high energy bands. Finally, our method doesn't work for transient class photons, because their background appears to depend on the spacecraft position. That is why we had to filter them out completely.

2.3 KS-test

We take care of remaining background by using the following functions with the Kolmogorov-Smirnov test:

$$\Phi_i(t) = \frac{p_i(T_1, t) - b_i \frac{t-T_1}{T_2-T_1}}{p_i(T_1, T_2) - b_i} \tag{1}$$

Here (T_1, T_2) is the time range of observations, $p_i(t_1, t_2)$ is the number of photons observed in the time range t_1 to t_2 in the i's energy band (i is either low or high for the low and high energy bands respectfully), and b_i is the estimated number of background photons for the time range T_1 to T_2 in the i's energy band.

The numbers of degrees of freedom (used as an input for the KS-test) are $p_i(T_1, T_2) - b_i$.

While we did not prove it, we assume that the Kolmogorov-Smirnov statistics computed for these functions with provided number of degrees of freedom has a similar distribution to that of the KS-statistics for ordinary CDFs (that is CDFs with no background).

Finally, we compute KS-probabilities for pairs $\Phi_{\text{low}}(t), \Phi_{\text{high}}(\kappa t)$ to obtain the allowed ranges for stretching factors κ. We evaluate stretching factors in the range $\texttt{STRETCHING\_MIN} = 0.1$ to $\texttt{STRETCHING\_MAX} = 10$. with a logarithmic step of $\texttt{STRETCHING\_STEP} = 1.001$.

As a result of such calculation we can constrain the range of allowed stretching factors to values for which the KS-probabilities are not too small, in other words, given the sigma-significance value, compute the range outside of which stretching factors are excluded by observations.

You can see the results of such computation in the following section.

2.4 Stretching factors

Out of 19 bursts studied, only 4 have at least 10 high energy events remaining after filtering, and thus eligible for computating the stretching factors. The results of this computation are shown on figures 3, 4, 5, 6 and table 2.

Out of these 4 bursts, two (GRB 080916C and GRB 090510) have stretching factors compatible with $\kappa = 1$ within 2σ range.

GRB 090926A has, however, high energy radiation stretched with respect to low energy radiation (that is $\kappa > 1$). In contrast to that, GRB 090902B has low energy radiation stretched with respect to high energy radiation ($\kappa < 1$).

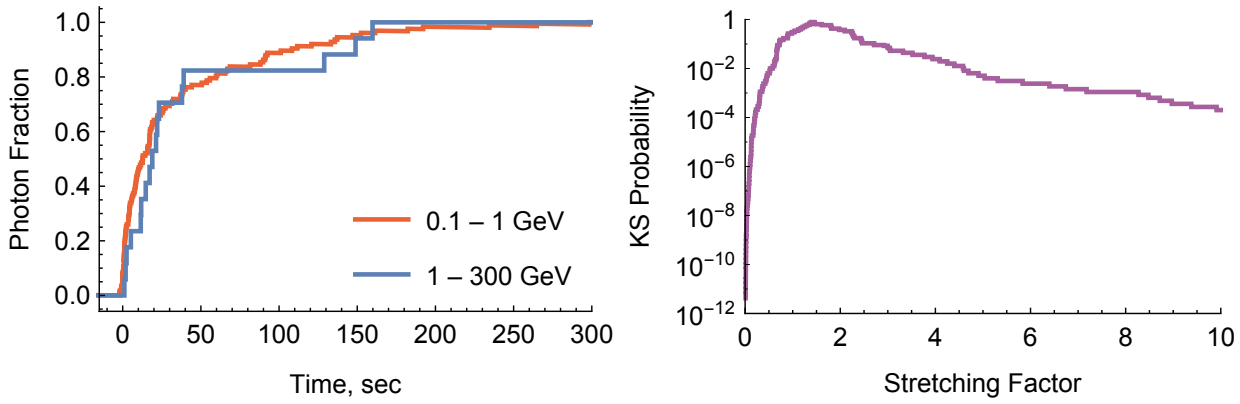

Figure 3: GRB 080916C results. Stretching factor is compatible with $\kappa = 1$ within 2σ.

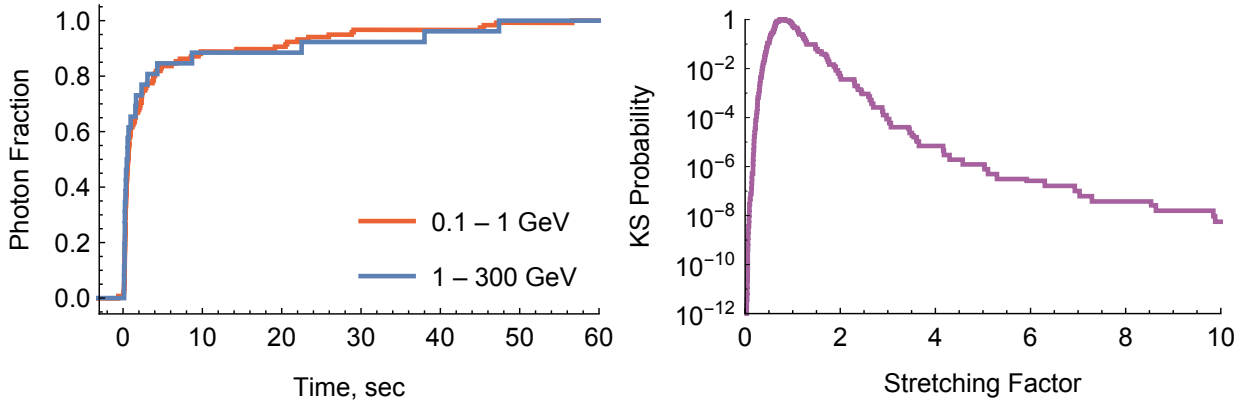

Figure 4: GRB 090510 results. Stretching factor is compatible with $\kappa = 1$ within 1σ.

So we obtained a preliminary (for significance is only 2σ) result that the stretching factors for observable bursts might be both larger and smaller than 1.

3 Model

3.1 Description

The main idea behind our model is to assume that the burst opening angle depends on energy of emitted photons, or, equivalently, that the most energetic plasma particles are concentrated near the axis of the jet, while low energy particles are on the periphery. As you can see on figure 1 this leads to a time stretching effect in some cases due to relativistic beaming.

At the moment, we do not have any rigorous proof of our assumption. There are arguments, however, supporting it.

First of all, the number of observed GRBs rapidly decreases with energy. There are around 750 bursts detected by GBM in hard X-rays and low energy gamma rays [1] (half of them were in a LAT field of view), only 30 or so were detected by LAT above 100 MeV, and only about 4 of them were detected above GeV. This observation is hard to explain in a framework of uniform jet model given that burst energetics are similar [3]. It is, however, easy to explain in our model, given that small observation angles are rare, and

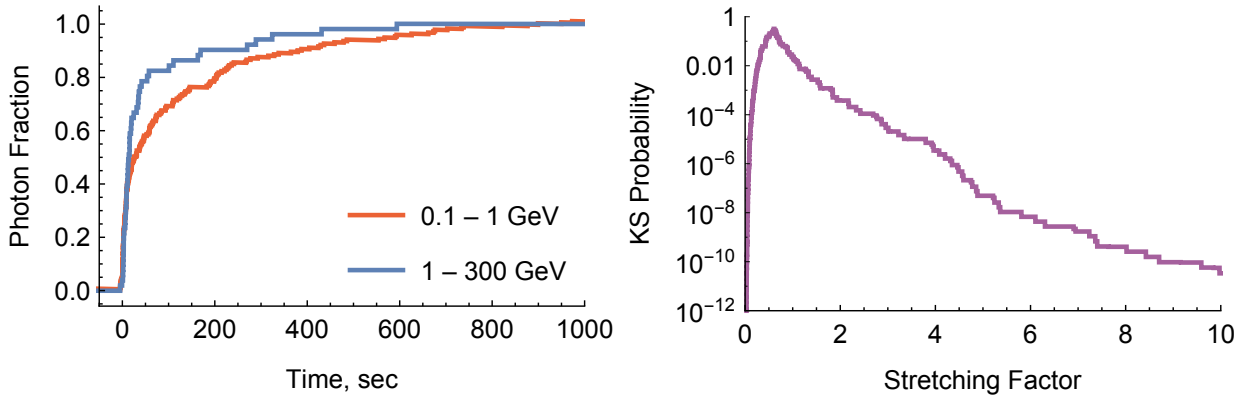

Figure 5: GRB 090902B results. Low energy radiation is stretched ($\kappa < 1$) with significance of 2.3σ.

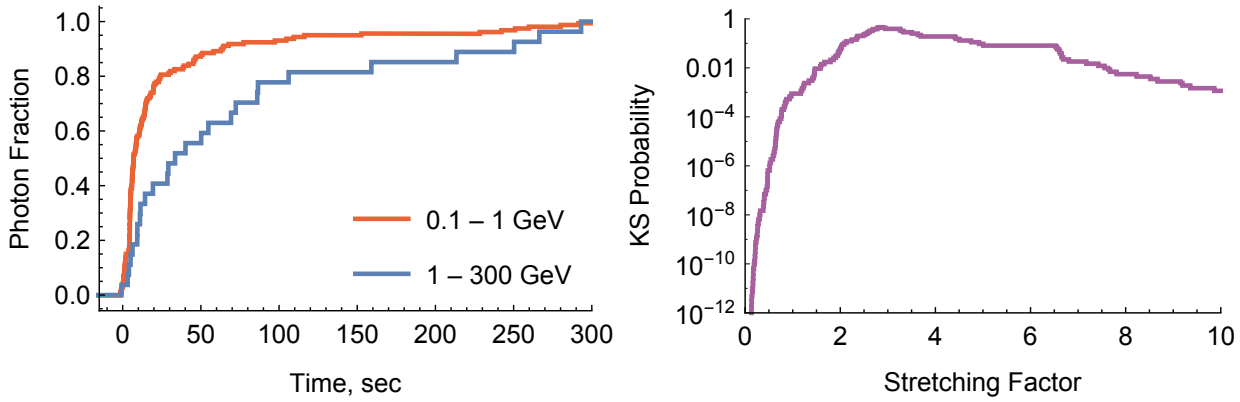

Figure 6: GRB 090926A results. High energy radiation is stretched ($\kappa > 1$) with significance of 3.3σ.

GRB	1σ	2σ	3σ	4σ	5σ
080916C	1.04 – 2.24	0.67 – 3.32	0.42 – 5.83	0.19 – 14.9	0.087 – 35.7
090501	0.58 – 1.1	0.43 – 1.61	0.32 – 2.29	0.22 – 3.03	0.17 – 5.11
090902B	0.604 – 0.613	0.35 – 0.89	0.22 – 1.53	0.13 – 2.86	0.078 – 4.49
090926A	2.61 – 3.33	1.99 – 6.62	1.34 – 9.15	0.73 – 13.5	0.48 – 19.4

Table 2: Burst observation results. Ranges of allowed stretching factors are shown for studied bursts for multiple levels of significance.

the only way to produce high energy radiation is to have the observation angle small enough.

Another argument comes from consideration of processes happening in jets, specifically the scattering of particles near the jet boundary. While plasma particles scatter, they simultaneously lose energy, and change directions, sometimes propagating beyond the jet boundary, and therefore increasing the jet opening angle. So, the processes of energy loss and increase of jet size are correlated, therefore the low energy particles should be closer to the jet boundary.

In the following sections we will rigorously derive the procedure for computing time stretching factors from our model, and compare them to observations obtained in the previous section.

3.2 Assumptions

To understand the observed spectral lag, lets explore geometry of the jet. First of all, lets make some assumptions:

1. Time $t = 0$, a spherical shell of plasma is emitted. The center is called the central engine.
2. The shell points propagate with a constant velocity $v = \frac{\sqrt{\gamma^2-1}}{\gamma} \sim 1$, so at the time t the radius of the shall is vt.
3. Each point of the shell is an isotropic radiator in its rest frame.
4. The radiation intensity is a function of the radiator position and the radiation frequency:

$$\eta(r,\theta,\omega) = \frac{\eta_0}{1+\left(\frac{r}{r_0}\right)^n} \exp\left(-\left(\frac{\theta}{\theta_0}\right)^2 \left(\frac{\omega}{\omega_0}\right)^{-2k}\right) \left(\frac{\omega}{\omega_0}\right)^{\alpha} \tag{2}$$

   η is a number of particles emitted per volume per solid angle per frequency. It is a function of the distance r from the central engine, of the off-axis angle θ, and of the radiation frequency ω.

The burst is fully specified by the following set of parameters:

- γ, the relativistic factor of the shell, $\gamma \gg 1$.
- η_0, which defines the luminosity scale.
- r_0, the characteristic jet length; $r_0 \ll \frac{1}{H(0)}$, $H(t)$ is the Hubble parameter;
- n, which determines the sharpness of the jet end, $n > 3$;
- ω_0, a characteristic radiation frequency;
- θ_0, the opening angle of the jet for radiation with frequency ω_0, $\theta_0 \ll 1$;
- k, which determines how much the opening angle changes with frequency, $k < 0$;
- α, the bare spectral index, $\alpha < -2k - 1$

Now we have all we need to calculate the observed light curves, and then the stretching factors.

3.3 Photon observation time

Lets begin by computing a time at which some particular photon is observed. This time is a function of the radiator location (r, θ, ϕ), as well as the observer location $(d, \chi, 0)$. (Here we choose coordinates so that the rotation angle of the observer is 0.) Lets assume for now that the observer is too far from the jet to resolve its geometry, yet close enough so that the expansion of space is negligible. This assumption allows us to ignore the effects of cosmology for this calculation.

The observation time is a sum of two terms: the time interval from $t = 0$ to the photon emission (the plasma time), and the time interval between the emission and the observation (the photon time):

$$t\left(r, \theta, \phi, d, \chi\right) = t_{\text{plasma}}\left(r\right) + t_{\text{photon}}\left(r, \theta, \phi, d, \chi\right)$$

t_{plasma} is easy to compute since plasma moves with uniform velocity:

$$t_{\text{plasma}}\left(r\right) = \frac{r}{v}$$

t_{photon} is a distance between the radiator and the observer:

$$\begin{aligned}
t_{\text{photon}}\left(r, \theta, \phi, d, \chi\right) &= \sqrt{\left(d\cos\chi - r\cos\theta\right)^2 + \left(d\sin\chi - r\sin\theta\cos\phi\right)^2 + \left(r\sin\theta\sin\phi\right)^2} \\
&= d\sqrt{\left(\cos\chi - \frac{r}{d}\cos\theta\right)^2 + \left(\sin\chi - \frac{r}{d}\sin\theta\cos\phi\right)^2 + \left(\frac{r}{d}\sin\theta\sin\phi\right)^2} \\
&\sim d\sqrt{\cos^2\chi - 2\frac{r}{d}\cos\theta\cos\chi + \sin^2\chi - 2\frac{r}{d}\sin\theta\cos\phi\sin\chi} \\
&\sim d\left(1 - \frac{r}{d}\left(\cos\theta\cos\chi + \sin\theta\cos\phi\sin\chi\right)\right) \\
&= d - r\left(\cos\theta\cos\chi + \sin\theta\cos\phi\sin\chi\right)
\end{aligned}$$

Combining these expressions together, we get:

$$t\left(r, \theta, \phi, d, \chi\right) = d + r\left(\frac{1}{v} - \cos\theta\cos\chi - \sin\theta\cos\phi\sin\chi\right)$$

Since no photon can reach the observer faster than the speed of light, and the photons emitted at $t = 0$ reach the observer at $t = d$, this time $t = d$ is the start of the observer's light curve. So we can define a more convenient time origin:

$$\tau\left(r, \theta, \phi, \chi\right) = t\left(r, \theta, \phi, d, \chi\right) - d = r\left(\frac{1}{v} - \cos\theta\cos\chi - \sin\theta\cos\phi\sin\chi\right)$$

Finally, we can use the spherical law of cosines to write this in terms of the great-circle distance $\sigma\left(\theta, \phi, \chi\right)$ between the points (θ, ϕ) and $(\chi, 0)$:

$$\tau\left(r, \theta, \phi, \chi\right) = r\left(\frac{1}{v} - \cos\sigma\left(\theta, \phi, \chi\right)\right) \tag{3}$$

Note that τ doesn't depend on d anymore. But this is only true if we did not account for cosmology, or if the scale factor did not change from emission to observation. For a distant observer it will change, however, which will stretch the distances between photons:

$$\tau\left(r, \theta, \phi, z, \chi\right) = r\left(\frac{1}{v} - \cos\sigma\left(\theta, \phi, \chi\right)\right)\left(1 + z\right) \tag{4}$$

Here z is the redshift of the burst from the point of view of the observer.

3.4 Light curve

We now know enough to compute the observable quantity - the number of observed photons p. For that we need to integrate the radiation intensity η over four things. Two burst-related things: radiator positions (r, θ, ϕ) and frequencies at emission ω'. Two observer-related things: observation time τ and frequencies at observation ω. We relate the first two and the second two with the delta functions:

$$\begin{aligned} p\left(z, \chi; \tau_1, \tau_2; \omega_1, \omega_2\right) = \frac{A_{\mathrm{det}}}{A_{\mathrm{ph}}\left(z\right)} \int_0^{\infty} \mathrm{d}r \int_0^{\pi} r \, \mathrm{d}\theta \int_0^{2\pi} r \sin\theta \, \mathrm{d}\phi \int_0^{\infty} \mathrm{d}\omega' \int_{\tau_1}^{\tau_2} \mathrm{d}\tau \int_{\omega_1}^{\omega_2} \mathrm{d}\omega \, \eta\left(r, \theta, \omega'\right) \\ \times \underbrace{\frac{1}{\gamma^2\left(1 - v\cos\sigma\left(\theta, \phi, \chi\right)\right)^2}}_{\text{aberration}} \underbrace{\frac{1}{\gamma\left(1 - v\cos\sigma\left(\theta, \phi, \chi\right)\right)}}_{\text{time dilation}} \\ \times \delta\left(\frac{\omega'}{\underbrace{\gamma\left(1 - v\cos\sigma\left(\theta, \phi, \chi\right)\right)}_{\text{relativistic shift}} \underbrace{\left(1 + z\right)}_{\text{cosmological shift}}} - \omega\right) \\ \times \delta\left(\tau - r\left(\frac{1}{v} - \cos\sigma\left(\theta, \phi, \chi\right)\right)\left(1 + z\right)\right) \end{aligned} \tag{5}$$

Here A_{det} is the effective area of the detector, and A_{ph} is an area of the sphere over which photons emitted in the burst are spread (see appendix B for derivation). We have taken account for four relativistic effects, which affect intensities and frequencies of the radiators: relativistic aberration; time dilation of the radiators relative to the observer; relativistic blue/redshift; and cosmological redshift.

We can use the delta functions to do the integrals over ω' and r. For that lets transform the first one:

$$\begin{aligned} \delta\left(\frac{\omega'}{\gamma\left(1 - v\cos\sigma\right)\left(1 + z\right)} - \omega\right) &= \delta\left(\frac{1}{\gamma\left(1 - v\cos\sigma\right)\left(1 + z\right)}\left(\omega' - \gamma\left(1 - v\cos\sigma\right)\left(1 + z\right)\omega\right)\right) \\ &= \gamma\left(1 - v\cos\sigma\right)\left(1 + z\right)\delta\left(\omega' - \gamma\left(1 - v\cos\sigma\right)\left(1 + z\right)\omega\right) \end{aligned}$$

And the second one:

$$\begin{aligned} \delta\left(\tau - r\left(\frac{1}{v} - \cos\sigma\right)\left(1 + z\right)\right) &= \delta\left(\left(\frac{1}{v} - \cos\sigma\right)\left(1 + z\right)\left(r - \frac{\tau}{\left(\frac{1}{v} - \cos\sigma\right)\left(1 + z\right)}\right)\right) \\ &= \frac{1}{\left(\frac{1}{v} - \cos\sigma\right)\left(1 + z\right)}\delta\left(r - \frac{\tau}{\left(\frac{1}{v} - \cos\sigma\right)\left(1 + z\right)}\right) \end{aligned}$$

After the transformations expression for p takes the following form:

$$\begin{aligned} p\left(z, \chi; \tau_1, \tau_2; \omega_1, \omega_2\right) = \frac{A_{\mathrm{det}}}{A_{\mathrm{ph}}\left(z\right)} \int_0^{\pi} \mathrm{d}\theta \int_0^{2\pi} \mathrm{d}\phi \int_{\tau_1}^{\tau_2} \mathrm{d}\tau \int_{\omega_1}^{\omega_2} \mathrm{d}\omega \\ \times \eta\left(\frac{\tau}{\left(\frac{1}{v} - \cos\sigma\left(\theta, \phi, \chi\right)\right)\left(1 + z\right)}, \theta, \gamma\left(1 - v\cos\sigma\left(\theta, \phi, \chi\right)\right)\left(1 + z\right)\omega\right) \\ \times \frac{\tau^2 \sin\theta}{\left(\frac{1}{v} - \cos\sigma\left(\theta, \phi, \chi\right)\right)^3\left(1 + z\right)^2\gamma^2\left(1 - v\cos\sigma\left(\theta, \phi, \chi\right)\right)^2} \\ = \frac{A_{\mathrm{det}}}{A_{\mathrm{ph}}\left(z\right)} \frac{1}{v^2\gamma^2\left(1 + z\right)^2} \int_{\tau_1}^{\tau_2} \mathrm{d}\tau \, \tau^2 \int_0^{\frac{\pi}{2}} \mathrm{d}\theta \int_0^{2\pi} \mathrm{d}\phi \int_{\omega_1}^{\omega_2} \mathrm{d}\omega \frac{\sin\theta}{\left(\frac{1}{v} - \cos\sigma\left(\theta, \phi, \chi\right)\right)^5} \end{aligned}$$

$$\times \eta\left(\frac{\tau}{\left(\frac{1}{v}-\cos\sigma\left(\theta,\phi,\chi\right)\right)\left(1+z\right)},\theta,\gamma\left(1-v\cos\sigma\left(\theta,\phi,\chi\right)\right)\left(1+z\right)\omega\right) \tag{6}$$

Furthermore, if we write η explicitly we can do the integrals over ω and τ:

$$\begin{aligned}
p\left(z,\chi;\tau_1,\tau_2;\omega_1,\omega_2\right) &= \frac{A_{\mathrm{det}}}{A_{\mathrm{ph}}\left(z\right)}\frac{1}{v^2\gamma^2\left(1+z\right)^2}\int_0^{\pi}\mathrm{d}\theta\int_0^{2\pi}\mathrm{d}\phi\int_{\omega_1}^{\omega_2}\mathrm{d}\omega\int_{\tau_1}^{\tau_2}\mathrm{d}\tau\,\tau^2\frac{\sin\theta}{\left(\frac{1}{v}-\cos\sigma\left(\theta,\phi,\chi\right)\right)^5}\\
&\quad\times\frac{\eta_0}{1+\left(\frac{\tau}{r_0\left(\frac{1}{v}-\cos\sigma\left(\theta,\phi,\chi\right)\right)\left(1+z\right)}\right)^n}\\
&\quad\times\exp\left(-\left(\frac{\theta}{\theta_0}\right)^2\left(\frac{\omega\gamma\left(1-v\cos\sigma\left(\theta,\phi,\chi\right)\right)\left(1+z\right)}{\omega_0}\right)^{-2k}\right)\\
&\quad\times\left(\frac{\omega\gamma\left(1-v\cos\sigma\left(\theta,\phi,\chi\right)\right)\left(1+z\right)}{\omega_0}\right)^{\alpha}\\
&= \frac{A_{\mathrm{det}}}{A_{\mathrm{ph}}\left(z\right)}\frac{\eta_0}{\left(v\gamma\left(1+z\right)\right)^{2-\alpha}}\int_0^{\pi}\mathrm{d}\theta\int_0^{2\pi}\mathrm{d}\phi\frac{\sin\theta}{\left(\frac{1}{v}-\cos\sigma\left(\theta,\phi,\chi\right)\right)^{5-\alpha}}\\
&\quad\times\int_{\omega_1}^{\omega_2}\mathrm{d}\omega\exp\left(-\left(\frac{\theta}{\theta_0}\right)^2\left(\frac{\omega\gamma\left(1-v\cos\sigma\left(\theta,\phi,\chi\right)\right)\left(1+z\right)}{\omega_0}\right)^{-2k}\right)\left(\frac{\omega}{\omega_0}\right)^{\alpha}\\
&\quad\times\int_{\tau_1}^{\tau_2}\mathrm{d}\tau\,\tau^2\frac{1}{1+\left(\frac{\tau}{r_0\left(\frac{1}{v}-\cos\sigma\left(\theta,\phi,\chi\right)\right)\left(1+z\right)}\right)^n}\\
&= \frac{A_{\mathrm{det}}}{A_{\mathrm{ph}}\left(z\right)}\frac{\eta_0}{\left(v\gamma\left(1+z\right)\right)^{2-\alpha}}\int_0^{\pi}\mathrm{d}\theta\int_0^{2\pi}\mathrm{d}\phi\frac{\sin\theta}{\left(\frac{1}{v}-\cos\sigma\left(\theta,\phi,\chi\right)\right)^{5-\alpha}}\\
&\quad\times\left(I\left(z,\chi,\omega_2;\theta,\phi\right)-I\left(z,\chi,\omega_1;\theta,\phi\right)\right)\left(J\left(z,\chi,\tau_2;\theta,\phi\right)-J\left(z,\chi,\tau_1;\theta,\phi\right)\right)
\end{aligned} \tag{7}$$

Here I and J are indefinite integrals over ω and τ:

$$I\left(z,\chi,\omega;\theta,\phi\right) = \frac{\omega\left(\frac{\omega}{\omega_0}\right)^{\alpha}E_{\frac{\alpha+1}{2k}+1}\left(\left(\frac{\theta}{\theta_0}\right)^2\left(\frac{\omega}{\omega_0}\right)^{-2k}\left(\gamma\left(1-v\cos\sigma\left(\theta,\phi,\chi\right)\right)\left(1+z\right)\right)^{-2k}\right)}{2k} \tag{8}$$

$$J\left(z,\chi,\tau;\theta,\phi\right) = \frac{\tau^3}{3}\,{}_2F_1\left(1,\frac{3}{n};\frac{n+3}{n};-\left(\frac{\tau}{r_0\left(\frac{1}{v}-\cos\sigma\left(\theta,\phi,\chi\right)\right)\left(1+z\right)}\right)^n\right) \tag{9}$$

where exponential integral function $E_n\left(x\right)=\int_1^{\infty}\frac{e^{-xt}\,\mathrm{d}t}{t^n}$.

The remaining integrals over θ and χ are hard to do symbolically, so we compute them numerically. To optimize this computation we can use the assumption of small θ and χ, so that:

$$\sin\theta\sim\theta$$

$$\cos\sigma\left(\theta,\phi,\chi\right)=\cos\theta\cos\chi+\sin\theta\sin\chi\cos\phi\sim 1-\frac{\theta^2}{2}-\frac{\chi^2}{2}+\theta\chi\cos\phi$$

Using this assumption, and the evenness of the integral as a function of θ, we arrive to the optimized expressions for p, I and J:

$$p\left(z,\chi;\tau_1,\tau_2;\omega_1,\omega_2\right) = \frac{A_{\mathrm{det}}}{A_{\mathrm{ph}}\left(z\right)}\frac{2\eta_0}{\left(v\gamma\left(1+z\right)\right)^{2-\alpha}}\int_0^{\infty}\mathrm{d}\theta\int_0^{\pi}\mathrm{d}\phi\frac{\theta}{\left(\frac{1}{v}-1+\frac{\theta^2}{2}+\frac{\chi^2}{2}-\theta\chi\cos\phi\right)^{5-\alpha}}$$

$$\times \left(I\left(z,\chi,\omega_2;\theta,\phi\right)-I\left(z,\chi,\omega_1;\theta,\phi\right)\right)\left(J\left(z,\chi,\tau_2;\theta,\phi\right)-J\left(z,\chi,\tau_1;\theta,\phi\right)\right) \tag{10}$$

$$I\left(z,\chi,\omega;\theta,\phi\right)=\frac{\omega\left(\frac{\omega}{\omega_0}\right)^{\alpha}E_{\frac{\alpha+1}{2k}+1}\left(\left(\frac{\theta}{\theta_0}\right)^2\left(\frac{\omega}{\omega_0}\right)^{-2k}\left(v\gamma\left(1+z\right)\left(\frac{1}{v}-1+\frac{\theta^2}{2}+\frac{\chi^2}{2}-\theta\chi\cos\phi\right)\right)^{-2k}\right)}{2k} \tag{11}$$

$$J\left(z,\chi,\tau;\theta,\phi\right)=\frac{\tau^3}{3}\,{}_2F_1\left(1,\frac{3}{n};\frac{n+3}{n};-\left(\frac{\tau}{r_0\left(\frac{1}{v}-1+\frac{\theta^2}{2}+\frac{\chi^2}{2}-\theta\chi\cos\phi\right)\left(1+z\right)}\right)^n\right) \tag{12}$$

Finally, we will need to compute limits of p for $\omega_2\to\infty$ and $\tau_2\to\infty$. It requires us to know the limit of I for $\omega\to\infty$ (we assumed that $k<0$):

$$I\left(z,\chi,\infty;\theta,\phi\right)=\lim_{\omega\to\infty}I\left(z,\chi,\omega;\theta,\phi\right)=0 \tag{13}$$

and the limit of J for $\tau\to\infty$ ($n>3$ by assumption):

$$J\left(z,\chi,\infty;\theta,\phi\right)=\lim_{\tau\to\infty}J\left(z,\chi,\tau;\theta,\phi\right)=\left(r_0\left(\frac{1}{v}-1+\frac{\theta^2}{2}+\frac{\chi^2}{2}-\theta\chi\cos\phi\right)\left(1+z\right)\right)^3\frac{\pi}{n\sin\frac{3\pi}{n}} \tag{14}$$

Now, when we know p, we can compute many different things with it. For example:

- the total number of particles observed in a given energy range, $p_\infty\left(z,\chi;\omega_1,\omega_2\right)=p\left(z,\chi;0,\infty;\omega_1,\omega_2\right)$;
- the fraction of photons observed during a given time interval, $\Phi\left(z,\chi;\tau_1,\tau_2;\omega_1,\omega_2\right)=\frac{p\left(z,\chi;\tau_1,\tau_2;\omega_1,\omega_2\right)}{p_\infty\left(z,\chi;\omega_1,\omega_2\right)}$;
- the duration of the burst $T_f\left(z,\chi;\omega_1,\omega_2\right)$, that is the time by which the fraction f of photons is observed. We can compute it by solving the following equation for T_f: $p\left(z,\chi;0,T_f;\omega_1,\omega_2\right)=fp_\infty\left(z,\chi;\omega_1,\omega_2\right)$;
- the stretching factor, which we will discuss in the next section.

3.5 Stretching factor

The stretching factor for a continuous light curve is defined exactly like the stretching factor for a discrete one. It is the value of κ which makes the KS-distance minimal:

$$\kappa\left(z,\chi;\omega_1,\omega_2,\omega_3\right)=\operatorname*{argmin}_{\kappa}\max_{\tau}\left|\Phi\left(z,\chi;0,\tau;\omega_1,\omega_2\right)-\Phi\left(z,\chi;0,\kappa\tau;\omega_2,\omega_3\right)\right| \tag{15}$$

The maximum of an absolute value cannot be differentiated, so the computation of κ by the given definition is complicated. Lets instead rewrite this expression in terms of a positive and a negative KS-distances:

$$\begin{aligned}
D_+\left(z,\chi;\kappa;\omega_1,\omega_2,\omega_3\right)&=\max_{\tau}\left(\Phi\left(z,\chi;0,\tau;\omega_1,\omega_2\right)-\Phi\left(z,\chi;0,\kappa\tau;\omega_2,\omega_3\right)\right)\\
D_-\left(z,\chi;\kappa;\omega_1,\omega_2,\omega_3\right)&=\min_{\tau}\left(\Phi\left(z,\chi;0,\tau;\omega_1,\omega_2\right)-\Phi\left(z,\chi;0,\kappa\tau;\omega_2,\omega_3\right)\right)\\
\kappa\left(z,\chi;\omega_1,\omega_2,\omega_3\right)&=\operatorname*{argmin}_{\kappa}\max\left(D_+\left(z,\chi;\kappa;\omega_1,\omega_2,\omega_3\right),-D_-\left(z,\chi;\kappa;\omega_1,\omega_2,\omega_3\right)\right)
\end{aligned}$$

Take note that Φ monotonously increases with τ. It implies that D_+ and D_- monotonously decrease with κ, so as $D_+ + D_-$. So there is a single value of κ, for which

$$D_+\left(z,\chi;\kappa;\omega_1,\omega_2,\omega_3\right)=-D_-\left(z,\chi;\kappa;\omega_1,\omega_2,\omega_3\right) \tag{16}$$

And this value of κ also makes the $\max(D_+, -D_-)$ minimal, since D_+ monotonously decrease, and $(-D_-)$ monotonously increase with κ.

So we have now a simpler way to compute κ by solving an equation instead of computing the minimum. And Φ can be differentiated, which makes it easier to compute maximums and minimums of their differences.

Being able to compute the stretching factor, we could now compare our model predictions with observations given the position of an observer. We don't know the observer's off-axis angle χ, however, so we cannot check the stretching factor prediction directly. Instead, we will focus on a series of tests, which will ensure that our model doesn't contradict existing observations. These tests will be discussed in the following sections.

3.6 Total energy

The first test is to compute the total energy radiated from the burst, and to ensure that it doesn't exceed the mass of the star from which the burst originated.

To compute the total energy, we need to multiply the radiation intensity by frequency, and integrate it over frequencies ω, volume (r, θ, ϕ), and observer positions (σ, ξ). We assumed $\theta \ll 1$, and have taken into account the same relativistic effects as we did in the observed particle count computation:

$$\begin{aligned} E &= \int_0^\infty \mathrm{d}\omega \int_0^\infty \mathrm{d}r \int_0^\infty r\,\mathrm{d}\theta \int_0^{2\pi} r\,\theta\,\mathrm{d}\phi \int_0^\infty \mathrm{d}\sigma \int_0^{2\pi} \sin\sigma\,\mathrm{d}\xi \\ &\quad \times \eta(r,\theta,\omega) \underbrace{\frac{1}{\gamma(1-v\cos\sigma)}}_{\text{time dilation}} \underbrace{\frac{1}{\gamma^2(1-v\cos\sigma)^2}}_{\text{aberration}} \underbrace{\frac{\omega}{\gamma(1-v\cos\sigma)}}_{\text{relativistic shift}} \\ &= \frac{4\pi^2}{\gamma^4} \int_0^\infty \mathrm{d}\omega\,\omega \int_0^\infty \mathrm{d}r\,r^2 \int_0^\infty \mathrm{d}\theta\,\theta\,\eta(r,\theta,\omega) \int_0^\infty \mathrm{d}\sigma \frac{\sin\sigma}{(1-v\cos\sigma)^4} \end{aligned} \tag{17}$$

An integral over σ is computable analytically:

$$\int_0^\infty \mathrm{d}\sigma \frac{\sin\sigma}{(1-v\cos\sigma)^4} = \frac{2\left(3+v^2\right)}{3\left(1-v^2\right)^3} = \frac{2}{3}\gamma^6\left(4-\frac{1}{\gamma^2}\right)$$

Substituting this result into the expression for E we get:

$$E = \frac{32\pi^2}{3}\left(\gamma^2-\frac{1}{4}\right)\int_0^\infty \mathrm{d}\omega\,\omega \int_0^\infty \mathrm{d}r\,r^2 \int_0^\infty \mathrm{d}\theta\,\theta\,\eta(r,\theta,\omega) \tag{18}$$

Now we can use the expression for η to do the remaining integrals:

$$E = \frac{32\pi^2\eta_0}{3}\left(\gamma^2-\frac{1}{4}\right)\int_0^\infty \mathrm{d}\omega\,\omega\left(\frac{\omega}{\omega_0}\right)^\alpha \int_0^\infty \mathrm{d}r\,\frac{r^2}{1+\left(\frac{r}{r_0}\right)^n} \int_0^\infty \mathrm{d}\theta\,\theta\,\exp\left(-\left(\frac{\theta}{\theta_0}\right)^2\left(\frac{\omega}{\omega_0}\right)^{-2k}\right)$$

The integrals over r and θ can be computed symbolically:

$$\int_0^\infty \mathrm{d}r\,\frac{r^2}{1+\left(\frac{r}{r_0}\right)^n} = \frac{\pi}{n\sin\left(\frac{3\pi}{n}\right)} r_0^3$$

$$\int_0^\infty \mathrm{d}\theta\,\theta\,\exp\left(-\left(\frac{\theta}{\theta_0}\right)^2\left(\frac{\omega}{\omega_0}\right)^{-2k}\right) = \frac{1}{2}\theta_0^2\left(\frac{\omega}{\omega_0}\right)^{2k}$$

Now we have only one integral left:

$$E = \frac{16\pi^3}{3n\sin\left(\frac{3\pi}{n}\right)}\left(\gamma^2-\frac{1}{4}\right)\eta_0\,r_0^3\,\theta_0^2\int_0^\infty \mathrm{d}\omega\,\omega\left(\frac{\omega}{\omega_0}\right)^{2k+\alpha} \tag{19}$$

Note, however, that since $\alpha < -2k - 1$ this integral diverges for $\omega \to 0$. But our model is not expected to describe low-energy radiation of the burst, so we should not integrate over low-frequency radiators. Nevertheless, we should ensure that the total energy of the high-energy radiation is not too large. To compute this energy we will only integrate over those radiators which emission we can observe, that is over the radiators with frequencies greater than $\frac{\omega_1}{\gamma}$, where ω_1 is the smallest observable photon frequency. Now we can compute the last integral and get the final expression for E:

$$\begin{aligned} E(\omega_1) &= \frac{16\pi^3}{3n\sin\left(\frac{3\pi}{n}\right)}\left(\gamma^2 - \frac{1}{4}\right)\eta_0\, r_0^3\, \theta_0^2 \int_{\frac{\omega_1}{\gamma}}^{\infty} \mathrm{d}\omega\, \omega \left(\frac{\omega}{\omega_0}\right)^{2k+\alpha} \\ &= \frac{16\pi^3}{3n\sin\left(\frac{3\pi}{n}\right)}\left(\gamma^2 - \frac{1}{4}\right)\eta_0\, r_0^3\, \theta_0^2 \frac{\omega_1^2 \left(\frac{\omega_1}{\gamma\omega_0}\right)^{2k+\alpha}}{\gamma^2(-2k-\alpha-2)} \\ &= \frac{16\pi^3}{3n\,(-2k-\alpha-2)\sin\left(\frac{3\pi}{n}\right)}\gamma^{-2k-\alpha}\left(1 - \frac{1}{4\gamma^2}\right)\eta_0\, r_0^3\, \theta_0^2 \frac{\omega_0^{-2k-\alpha}}{\omega_1^{-2k-\alpha-2}} \end{aligned} \tag{20}$$

This energy should not be larger than a typical mass M_s of a massive star. So, finally, we arrive at the first constraint for the burst parameters:

$$\frac{16\pi^3}{3n\,(-2k-\alpha-2)\sin\left(\frac{3\pi}{n}\right)}\gamma^{-2k-\alpha}\left(1 - \frac{1}{4\gamma^2}\right)\eta_0\, r_0^3\, \theta_0^2 \frac{\omega_0^{-2k-\alpha}}{\omega_1^{-2k-\alpha-2}} < M_s \tag{21}$$

3.7 Distribution of stretching factors

The second test is to calculate the distribution of stretching factors of observable bursts, and to compare it to observations.

The computation of the exact and precise distribution is technically hard (because stretching factors change monotonously neither with redshifts, nor with off-axis angles), and computationally intensive. So we will not compute the precise distribution.

Instead, we will use the Monte-Carlo method to produce a large representative sample of stretching factors. Then, we will calculate an empirical CDF of this sample, which can be compared with observations using the KS-test. Since we can compute much larger sample than that of observations, we will not lose much precision due to this simplification.

We still have one ingredient missing though – the evolution of the bursts density. We assume that the bursts density is roughly proportional to the stars density, and the stars density is roughly proportional to the matter density, which changes with z as $(1+z)^3$. It is clear, however, that since no stars existed at very small redshifts, the burst density should decline there, so we add an exponential cutoff to it:

$$\rho = \rho_0 (1+z)^3 \exp\left(-\frac{z}{z_c}\right) \tag{22}$$

Here ρ_0 is a normalization factor, and z_c is a redshift scale, after which the density is cut off.

Now when we have all the ingredients, we can compute the sample with the following steps:

1. First of all we need to define the range from which to select redshifts and off-axis angles. We should include all observable jet positions in this range. However, to avoid dropping too many points corresponding to invisible bursts, we should keep the range as small as possible. We also want to make the region rectangular to be able to select redshifts and angles separately.

   Lets start by selecting a range for redshifts. Ideally, we want this range to start with $z = 0$. Then, however, there will be visible jets for all possible off-axis angles, which will make our angles range too large. Note also, that since the bursts count increases with redshift as z^3, the probability to observe a low-redshift burst is very small. So instead of selecting the smallest redshift to be 0, we select it to be a small number $z_{\min}$.

$z_{\max}$ is defined by the farthest jet, which can be observed. Since the burst observability $p_\infty(z, \chi; \omega_2, \omega_3)$ decreases with both redshift and χ, we can find the maximum redshift by solving the following equation:

$$p_\infty(z_{\max}, 0; \omega_2, \omega_3) = p_{\min} \tag{23}$$

where $p_{\min}$ is the minimum number of particles required to claim an observation.

2. The range for off-axis angles is easier to compute since nothing prohibits us from selecting the smallest angle to be 0.

   The observability declines with z and χ, so the observable burst with the largest χ should be located at the redshift $z_{\min}$. We can find this angle by solving the similar equation, as we did for the redshifts:

$$p_\infty(z_{\min}, \chi_{\max}; \omega_2, \omega_3) = p_{\min} \tag{24}$$

3. Now we are in a position to select a particular properly distributed random redshift. The CDF of the distribution of redshifts is a ratio of redshift counts in different space volumes:

$$\Phi_z(z) = \frac{\int_{z_{\min}}^{z} \rho(z')\, \mathrm{d}V(z')}{\int_{z_{\max}}^{z_{\max}} \rho(z')\, \mathrm{d}V(z')} \tag{25}$$

   where $\mathrm{d}V(z')$ is the volume of the infinitesimal shell surrounding a sphere over which bursts at redshift z' are distributed (see appendix B for derivation).

   To generate a redshift, we should uniformly select a value of Φ_z, and solve the corresponding equation for z:

$$\Phi_z(z) = x \tag{26}$$

   where x is a random variable uniformly distributed in the range 0 to 1.

4. An off-axis angle can be selected in a similar way. The CDF of the angles distribution is a ratio of spherical areas:

$$\Phi_\chi(\chi) = \frac{\int_0^{\chi} \sin\chi'\, \mathrm{d}\chi'}{\int_0^{\chi_{\max}} \sin\chi'\, \mathrm{d}\chi'} \approx \frac{\int_0^{\chi} \chi'\, \mathrm{d}\chi'}{\int_0^{\chi_{\max}} \chi'\, \mathrm{d}\chi'} = \left(\frac{\chi}{\chi_{\max}}\right)^2 \tag{27}$$

   As with redshifts, we get a properly distributed χ by solving the equation:

$$\Phi_\chi(\chi) = \left(\frac{\chi}{\chi_{\max}}\right)^2 = y \tag{28}$$

$$\chi = \chi_{\max}\sqrt{y} \tag{29}$$

   Here y is an another independent random variable uniformly distributed in the range 0 to 1.

5. Now we should check, if the burst in a selected position can be observed: $p_\infty(z, \chi; \omega_2, \omega_3) > p_{\min}$. If it is, add $\kappa(z, \chi)$ to the sample. If not, repeat from the step 3.

6. If the sample is not as big as we want yet, repeat from the step 3.

With this algorithm, we arrive to our second test / constraint for the burst parameters. The obtained stretching factors distribution should be compatible with observations.

3.8 High energy bursts fraction

Our final test is comparison of answers to this question: given the bursts which were observed in a whole energy range (ω_1, ω_3), which fraction of them can also be observed in a high energy range (ω_2, ω_3)?

To calculate this value, we need to compute the number of bursts visible in a given energy range, which is the integral over space and jet directions:

$$\begin{aligned} b(\omega_1, \omega_2) &= \int_0^{z_{\max}(\omega_1,\omega_2)} \mathrm{d}V(z)\,\rho(z) \int_0^{\chi_{\max}(z,\omega_1,\omega_2)} 2\pi \sin\chi \,\mathrm{d}\chi \\ &\approx 2\pi \int_0^{z_{\max}(\omega_1,\omega_2)} \mathrm{d}V(z)\,\rho(z) \int_0^{\chi_{\max}(z,\omega_1,\omega_2)} \chi \,\mathrm{d}\chi = \pi \int_0^{z_{\max}(\omega_1,\omega_2)} \mathrm{d}V(z)\,\rho(z)\,\chi^2_{\max}(z,\omega_1,\omega_2) \end{aligned} \tag{30}$$

Here $z_{\max}(\omega_1, \omega_2)$ and $\chi_{\max}(z, \omega_1, \omega_2)$ are the same values we used in the previous section: the maximum redshift from which a burst can be observed in a given energy range, and the maximum off-axis angle with which the burst at redshift z can be observed.

The fraction we want to compute is the ratio of these integrals:

$$f(\omega_1, \omega_2, \omega_3) = \frac{b(\omega_2, \omega_3)}{b(\omega_1, \omega_3)} = \frac{\int_0^{z_{\max}(\omega_2,\omega_3)} \mathrm{d}V(z)\,\rho(z)\,\chi^2_{\max}(z,\omega_2,\omega_3)}{\int_0^{z_{\max}(\omega_1,\omega_3)} \mathrm{d}V(z)\,\rho(z)\,\chi^2_{\max}(z,\omega_1,\omega_3)} \tag{31}$$

This is our 3rd test – the ratio obtained should be compatible with the observed value.

4 Results

4.1 Parameter fit

For now we discussed how to compute various observables of the model, and how to test the model against the data from observations. However, we never considered specific values for parameters of the burst. We will do that in this section.

First of all, we need to determine, which parameters to fit. At most, the observables of a particular burst depend on 10 parameters: 8 of the burst $(\gamma, \eta_0, r_0, n, \omega_0, \theta_0, k, \alpha)$, and 2 of the observer (z, χ). However, some of these parameters only change observables trivially, and, also, there are transformations of variables, which will not change observables at all (see equation 10):

- The number of photons p depends linearly on η_0, so η_0 doesn't affect other observables like duration, or stretching factor. We can easily fit η_0 to match the observed photon count.
- If we make a simultaneous transformation of $r_0 \to \lambda r_0$ and $\eta_0 \to \frac{1}{\lambda^3}\eta_0$, where λ is a parameter of transformation, only duration of the burst will change. Other observables, like the total number of photons, or stretching factor, will not be affected.
- Finally, if we make a following transformation: $\omega_0 \to \lambda\omega_0$, $\theta_0 \to \lambda^k\theta_0$, $\eta_0 \to \lambda^\alpha\eta_0$, where λ is another transformation parameter, no observables will change whatsoever.

Given these transformations, we can reduce the number of parameters for fit to 7: $(\gamma, n, \theta_0, k, \alpha, z, \chi)$.

Also, some of these parameters we know from observations:

- Redshifts z of many bursts have been measured [8].
- We know that relativistic factors γ are on the order of magnitude[4] of $\gamma = 300$ [17].

[4] Our minimization procedure can find similar minimums for other values of γ, at least from 100 to 1000

This knowledge allows us to reduce the number of parameters to minimize against to just 5: $(n, \theta_0, k, \alpha, \chi)$.

We want our cost function $C(n, \theta_0, k, \alpha, \chi)$ to satisfy the following objectives:

- Total energy of the burst is finite (that is $k + \frac{\alpha}{2} + 1 < 0$) and smaller than $6 \times 10^{53}\,\mathrm{GeV} \approx 10^{51}\,\mathrm{erg}$ [2].
- The stretching factor of the burst should be compatible with the value for the GRB 090926A.
- We require all bursts to have the same burst parameters $(\gamma, \eta_0, r_0, n, \omega_0, \theta_0, k, \alpha)$. And we know that bursts with small stretching factors like GRB 090902B should be possible to observe. So we require that bursts with the stretching factor of GRB 090902B or lower appear in random samples by z and χ (sampling is done the same way as in section 3.7).
- The ratio of photons with high energies and low energies should be compatible with the value for the GRB 090926A, $\frac{p_\infty(z,\chi;1\,\mathrm{GeV},\infty)}{p_\infty(z,\chi;0.1\,\mathrm{GeV},1\,\mathrm{GeV})} = 0.057$.
- Finally, the burst should not be too faint compared to other bursts from the sample. In other words, the total number of observed photons should approximately equal to the median among the sample.

The cost function is then computed by the following procedure:

1. Set $\gamma = 300$, $\omega_0 = 1\,\mathrm{GeV}$, $z = 2.1062$ (which is the redshift of GRB 090926A)
2. Set η_0 and r_0 such that the duration of the burst, and the total number of observed photons are compatible with GRB 090926A, $T_{0.99}(z, \chi; 0.1\,\mathrm{GeV}, \infty) = 219.5\,\mathrm{sec}$ and $p_\infty(z, \chi; 0.1\,\mathrm{GeV}, \infty) = 179.996$
3. If $k + \frac{\alpha}{2} + 1 < 0$, or the energy of the burst $E(0.1\,\mathrm{GeV}) > 6 \times 10^{53}\,\mathrm{GeV}$, the cost function equals to the penalization factor: $C(n, \theta_0, k, \alpha, \chi) = 400$.
4. Compute the small sample of 10 bursts (we will need stretching factors and total photon counts) with the same fixed burst parameters $(\gamma, \eta_0, r_0, n, \omega_0, \theta_0, k, \alpha)$, and with z and χ representatively distributed (as discussed in section 3.7).
5. Compute the cost due to the stretching factor:
$$C_\kappa = \frac{\log \kappa(z, \chi; 0.1\,\mathrm{GeV}, 1\,\mathrm{GeV}, \infty) - \log \kappa_{\mathrm{GRB090926A}}}{\Delta \log \kappa_{\mathrm{GRB090926A}}} \tag{32}$$
Here $\log \kappa_{\mathrm{GRB090926A}} = \frac{1}{2}\big(\log(6.62) + \log(1.99)\big)$ and $\Delta \log \kappa_{\mathrm{GRB090926A}} = \frac{1}{2}\big(\log(6.62) - \log(1.99)\big)$.
6. Compute the cost due to the minimal stretching factor from the sample:
$$C_{\kappa\mathrm{min}} = \max\left(0, \frac{\log \kappa_{\mathrm{min}} - \log \kappa_{\mathrm{GRB090902B}}}{\Delta \log \kappa_{\mathrm{GRB090902B}}}\right) \tag{33}$$
Here κ_{min} is the minimal stretching factor from the sample computed in the step 4, $\log \kappa_{\mathrm{GRB090902B}} = \frac{1}{2}\big(\log(0.89) + \log(0.35)\big)$ and $\Delta \log \kappa_{\mathrm{GRB090902B}} = \frac{1}{2}\big(\log(0.89) - \log(0.35)\big)$.
7. Compute the cost due to the fraction of high and low energy photon counts:
$$C_f = \frac{\log \frac{p_\infty(z,\chi;1\,\mathrm{GeV},\infty)}{p_\infty(z,\chi;0.1\,\mathrm{GeV},1\,\mathrm{GeV})} - \log f_{\mathrm{GRB090926A}}}{\log(10)} \tag{34}$$
Here $f_{\mathrm{GRB090926A}} = 0.0570003$.
8. Compute the cost due to the brightness of the burst compared to the median:
$$C_b = \frac{\log \frac{p_\infty(z,\chi;0.1\,\mathrm{GeV},\infty)}{p_{\mathrm{med}}} - 0}{\log(10)} \tag{35}$$
Here p_{med} is the median number of observed photons among the sample computed in the step 4.

n	θ_0	k	α	χ
22.1525	2.16424×10^{-4}	$-0.417\,021$	$-1.351\,630\,0$	7.04982×10^{-3}
25.8640	4.90222×10^{-8}	$-2.908\,750$	$3.538\,010\,0$	2.86570×10^{-4}
17.5380	1.46284×10^{-3}	$-2.133\,600$	$-2.133\,600\,0$	1.52624×10^{-3}
17.9736	4.52631×10^{-6}	$-1.402\,620$	$-0.011\,413\,2$	3.25900×10^{-4}
5.0000	1.12535×10^{-7}	$-0.200\,000$	$-2.000\,000\,0$	4.73795×10^{-3}
7.0000	2.00000×10^{-12}	$-3.000\,000$	$-3.000\,000\,0$	1.73795×10^{-3}

Table 3: Initial points used for minimization procedure from section 4.1.

9. Finally, the value of the cost function is the sum of squares of the four:

$$C = C_\kappa^2 + C_{\kappa\min}^2 + C_f^2 + C_b^2 \tag{36}$$

We use the Nelder-Mead (downhill simplex) method for the minimization procedure. Initial points were chosen to include the areas in parameter space where each cost is close to 0 (first 4 points correspondingly), and to cover the large fraction of the parameter space. You can see the values in table 3.

The minimization then converged to the following parameter values:

- $\gamma = 300$
- $\eta_0 = 4.629640817921788 \times 10^{34}\,\mathrm{sec}^{-3}\mathrm{GeV}^{-1}$
- $r_0 = 3.142715108207946 \times 10^6\,\mathrm{sec}$
- $\boldsymbol{n = 22.9977}$
- $\omega_0 = 1\,\mathrm{GeV}$
- $\boldsymbol{\theta_0 = 7.93393 \times 10^{-5}}$
- $\boldsymbol{k = -0.65356}$
- $\boldsymbol{\alpha = -0.724394}$
- $z = 2.1062$
- $\boldsymbol{\chi = 0.00590163}$

Note, that these parameter values (except for z and χ) are universal, and they can describe the whole population of observed bursts, as will be shown in the next section.

4.2 Results of the tests

As was discussed in the previous section our model can reproduce both stretching factors smaller than 1 (like of GRB 090902B) and larger than 1 (like of GRB 090926A) depending on redshift and observer's off-axis angle (see fig. 2).

Here are results of our tests:

- Total energy emitted in 100 MeV and more energetic gamma rays $E < 5.89 \times 10^{53}\,\mathrm{GeV}$, which is in agreement with [2].
- The distribution of observable bursts' stretching factors is shown on fig. 7. This distribution does not contradict to the values of stretching factors obtained in section 2.
- The fraction of bursts observable in low energy band, which are also observed in high energy band $f_m = 0.110$. The Fermi LAT catalog contains 35 bursts out of which 4 can be observed in high energy band. Therefore the observed value $f_o = 0.11 \pm 0.05$ (error obtained from binomial distribution) agrees with the model.

Also, there is a correlation between the fraction of high energy photons (that is high energy photon count divided by the total photon count), the stretching factor and the observer's off-axis angle (see fig. 8). It allows one to predict observer's off-axis angles.

So our model is able to explain the time stretching effect from section 2.

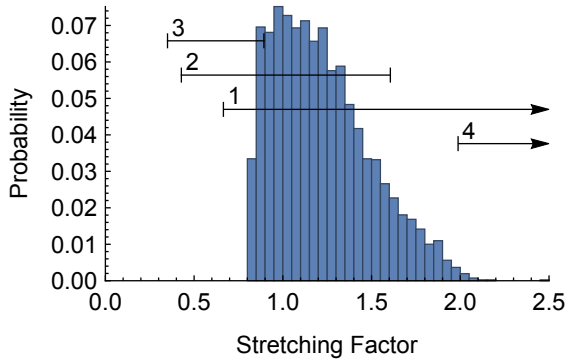

(a) Histogram (blue) obtained from the model. Black error bars show observed stretching factors.

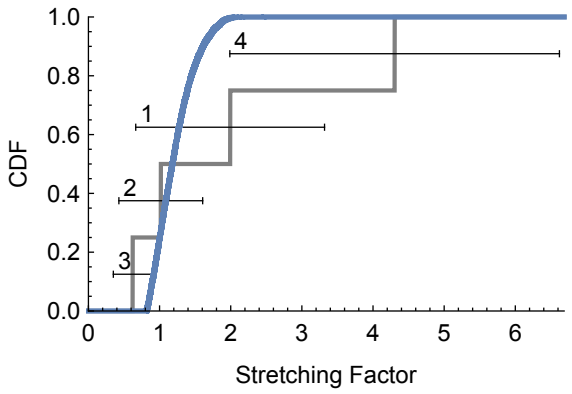

(b) CDF (blue) obtained from the model. Gray curve and black error bars show observed stretching factors.

Figure 7: Stretching factors histogram and CDF produced by our model. The sample contains 4096 bursts. Numbered error bars correspond to GRB 080916C, GRB 090510, GRB 090902B and GRB 090926A (in this order).

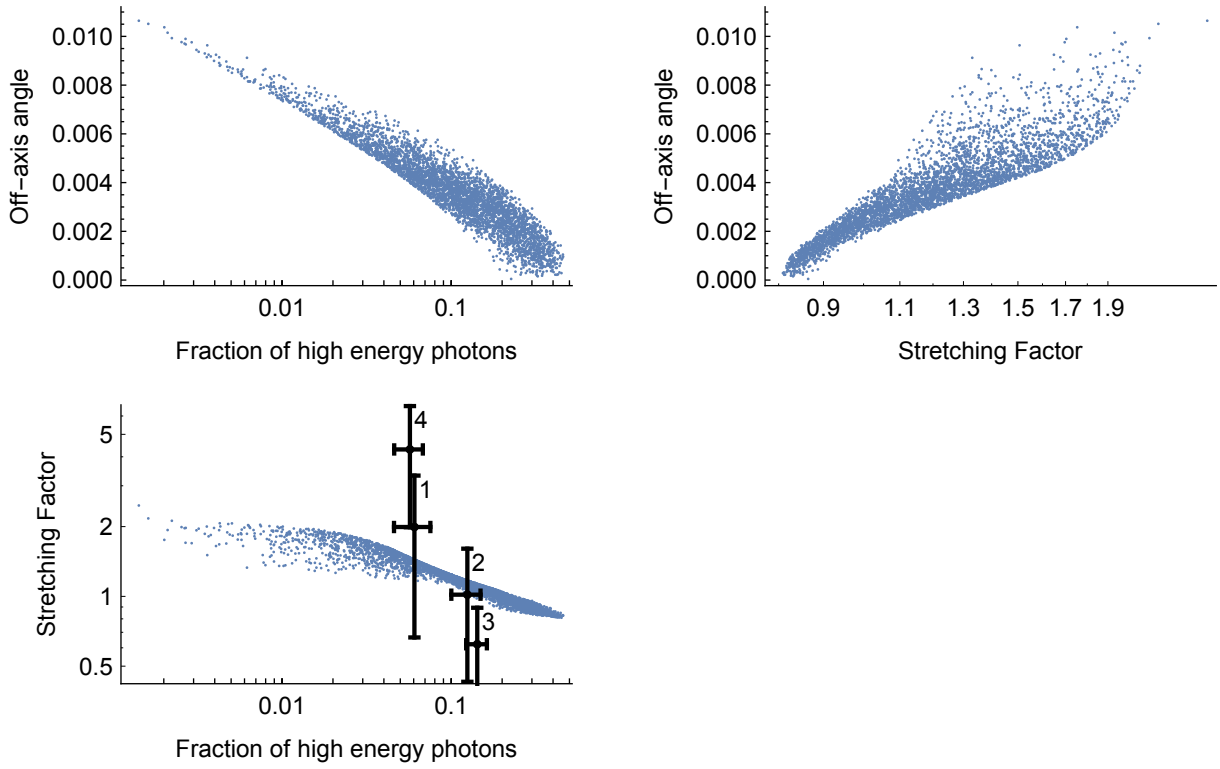

Figure 8: Correlations between off-axis angles, stretching factors and high to low energy photon count ratios found in the sample produced by our model. The sample contains 4096 bursts. Numbered black crosses show data for GRB 080916C, GRB 090510, GRB 090902B and GRB 090926A (in this order) with 2σ error bars. This correlation allows one to estimate off-axis angles of observed bursts.

5 Summary

Our study can be summarized with 3 main conclusions.

First, the time stretching of GRB light curves between different VHE (in particular $(100\,\mathrm{MeV}, 1\,\mathrm{GeV})$ and $(1\,\mathrm{GeV}, 300\,\mathrm{GeV})$) bands is discovered with statistic significance of 3.3σ. This time stretching might be positive or negative (that is higher or lower energy light curve is stretched) depending on the burst.

Second, this time stretching effect can be explained with curvature effects, that is effects of jet geometry. There is no need to introduce any new spectral components.

Finally, we can assume all GRBs to be the same in their rest frames. The internal burst parameters (such as γ, η_0, r_0, n, ω_0, θ_0, k and α) might stay the same for all bursts, and this assumption is more or less consistent with existing observations.

However, there are some caveats, and directions for improvement.

First of all, the model prediction and observations are not completely consistent. If you look at fig. 8, you will see that the stretching factor of GRB 090926A is too high compared to the model prediction. It appears that parameters of the model cannot be fitted to account for it (without ruining agreement with other observations). More data should be analyzed to see whether the problem will be exacerbated, and some refinement of the model might also be required.

Second, the shapes of light curves produced by the model (see fig. 2) differ considerably from observed ones (e.g. fig. 5). Most importantly, the slope of light curves produced by the model is zero at $t = 0$, even though the slope of observed light curves at $t = 0$ is not only non-zero, but appears to have a maximum.

Third, the assumption of plasma energy dependence on off-axis angle should be better justified. This might probably be done using hydrodynamic simulation of the jet.

Finally, even though it appears that bursts are similar in their rest frames, they cannot be exactly the same. The differences in masses, metallicities, angular momenta of progenitor stars, and the differences in local conditions around them might account for differences in light curves of GRBs (or, even, for especially large stretching factor of GRB 090926A). It means that minor variations of model parameters might be necessary on burst per burst basis.

It seems, however, that all these problems are not unresolvable, and may be addressed by refining the model without changing its main assumptions.

Acknowledgments. The work was supported by Russian Science Foundation grant 14-12-01340.

A Details of using Fermi Science tools

This appendix contains two things: exact values we are passing to a web form on the Fermi LAT data server, and the code we use to invoke the Fermi tools (including full list of options).

Parameters that are passed to the web form of the Fermi LAT data server to download the bursts data are the following:

- **Object name or coordinates**. Coordinates are filled from the table 1.
- **Coordinate system**. J2000.
- **Search radius (degrees)**. 60. Events are filtered by location separately by using the point spread functions (PSFs) of the LAT (as described in section 2.1).
- **Observation dates**. To have a decent safety margin, we extend the duration of the burst by 50% to both past and future relative to the table 1 time ranges. So, we fill in the following values:

$$\begin{aligned} &\texttt{time} + \texttt{startOffset} - 0.5\,(\texttt{endOffset} - \texttt{startOffset})\,, \\ &\texttt{time} + \texttt{endOffset} + 0.5\,(\texttt{endOffset} - \texttt{startOffset}) \end{aligned}$$

- **Time system**. MET.

- **Energy range (MeV)**. 100, 300000. This includes our both energy ranges.
- **LAT data type**. Extended.
- **Spacecraft data**. Checked. It is required for both events filtering, and calculation of the PSFs and exposure maps.

For background, all parameters are the same, except for the time ranges, which are the following:

$$\texttt{time} + \texttt{startOffset} - 0.5\,(\texttt{endOffset} - \texttt{startOffset}) - 86400,$$
$$\texttt{time} + \texttt{startOffset} - 0.5\,(\texttt{endOffset} - \texttt{startOffset})$$

The commands we use to invoke Fermi Science tools are the following:

```
gtselect infile=[eventFile] outfile=filtered.fits
       ra=INDEF dec=INDEF rad=180 tmin=INDEF tmax=INDEF emin=100 emax=300000
       zmax=100 evclass=2 convtype=-1 evtable=EVENTS
```

Here `[eventFile]` is the file downloaded from the Fermi LAT data server.

```
gtmktime scfile=[spacecraft] sctable=SC_DATA
       filter="DATA_QUAL>0 && LAT_CONFIG==1" roicut=yes
       evfile=filtered.fits evtable=EVENTS outfile=timed.fits
       apply_fiter=yes
```

where `[spacecraft]` is the FITS file containing the spacecraft data (also downloaded from the Fermi LAT data server).

```
gtltcube evfile=timed.fits evtable=EVENTS scfile=[spacecraft] sctable=SC_DATA
       outfile=ltcube.fits
       dcostheta=0.025 binsz=1 phibins=0 tmin=0 tmax=0 zmax=100 zmin=0

gtpsf expcube=ltcube.fits outfile=psf_[IrfName].fits outtable=PSF irfs=[IrfName]
       ra=[RA] dec=[DEC] emin=100 emax=300000 nenergies=41 thetamax=30 ntheta=300
```

`[RA]` and `[DEC]` here are the coordinates of the burst, and `[IrfName]` is the Instrument Response Function, which depends on photon's event class (transient, source, clean, or ultraclean) and conversion type (back or front). The list of IRF names can be obtained with the `gtirfs` tool. We need to compute PSFs for all of them.

```
gtexpcube2 infile=ltcube.fits cmap=none outfile=expcube_[IrfName].fits irfs=[IrfName]
       nxpix=360 nypix=180 binsz=1 coordsys=CEL xref=0 yref=0 axisrot=0
       proj=CAR ebinalg=log emin=100 emax=300000 enumbins=40
       ebinfile=NONE bincalc=EDGE ignorephi=no thmax=180 thmin=0 table=Exposure
```

Note, that R.A. coordinates in the `expcube` FITS files are indexed in reverse order and starting from 180. For example, `ra[0]` = 180, `ra[1]` = 179, and so on.

B Cosmology

This appendix contains a few formulas we need from cosmology, in particular the area of a photon sphere $A_{\mathrm{ph}}(z)$, a sphere over which photons emitted in a particular burst at redshift z are spread; and the volume of the infinitesimal shell surrounding a burst sphere $\mathrm{d}V(z)$, a sphere over which bursts at redshift z are distributed.

First of all, the metric of the expanding Universe:

$$\mathrm{d}s^2 = -\,\mathrm{d}t^2 + a^2(t)\,\mathrm{d}r^2 + a^2(t)\,r^2\,\mathrm{d}\Omega_2 \tag{37}$$

We define $a(t_{\text{obs}}) = 1$, where t_{obs} is the observation time.

We need to understand how the scale factor changes with time. For that we assume that the energy content of the Universe consists of matter Ω_m and vacuum energy Ω_Λ only, so that the Friedmann equation takes the following form:

$$\left(\frac{\dot{a}(t)}{a(t)}\right)^2 = \Omega_m H_{\text{obs}}^2 \frac{1}{a^3(t)} + H_{\text{obs}}^2 \Omega_\Lambda$$

$$\dot{a}(t) = a(t) H_{\text{obs}} \sqrt{\Omega_m \frac{1}{a^3(t)} + \Omega_\Lambda}$$

$$\mathrm{d}t = \frac{\mathrm{d}a}{a(t) H_{\text{obs}} \sqrt{\Omega_m \frac{1}{a^3(t)} + \Omega_\Lambda}}$$

Here $H_{\text{obs}} = H(t_{\text{obs}}) = \frac{\dot{a}(t_{\text{obs}})}{a(t_{\text{obs}})} = \dot{a}(t_{\text{obs}})$ is the Hubble parameter at the observation time.

We also need to know the areas of two spheres: the photon sphere, a sphere over which photons emitted in a particular burst are spread; and the bursts sphere, a sphere over which bursts at a particular redshift are distributed. These two spheres have the same radii – a distance from the observer to the burst, but different centers: the photon sphere is centered on the burst, while the bursts sphere is centered on the observer. Also, they have different areas, because the scale factor differs at locations of burst and observer.

Lets begin with the photon sphere. This sphere has the origin at $r = 0$ and $t = 0$, at the central engine of a particular burst. Taking $\mathrm{d}s = 0$ and $\mathrm{d}\Omega_2 = 0$ in the equation for metric, we get:

$$\mathrm{d}r = \frac{\mathrm{d}t}{a(t)}$$

And now we integrate over time to find the observer's position:

$$\begin{aligned} r(t_{\text{obs}}) &= \int_0^{t_{\text{obs}}} \frac{\mathrm{d}t}{a(t)} \\ &= \int_{a(0)}^{1} \frac{\mathrm{d}a}{a^2(t) H_{\text{obs}} \sqrt{\Omega_m \frac{1}{a^3(t)} + \Omega_\Lambda}} \\ &= \frac{{}_2F_1\left(\frac{1}{3}, \frac{1}{2}; \frac{4}{3}; -\frac{\Omega_m}{a^3(0)\Omega_\Lambda}\right) - a(0)\ {}_2F_1\left(\frac{1}{3}, \frac{1}{2}; \frac{4}{3}; -\frac{\Omega_m}{\Omega_\Lambda}\right)}{a(0) H_{\text{obs}} \sqrt{\Omega_\Lambda}} \end{aligned}$$

Here ${}_2F_1(a, b; c; z) = \frac{\Gamma(c)}{\Gamma(b)\Gamma(c-b)} \int_0^1 \frac{t^{b-1}(1-t)^{c-b-1}}{(1-tz)^a}\,\mathrm{d}t$ is a hypergeometric function. We can substitute $a(0) = \frac{1}{1+z}$, so, finally,

$$r(z) = \frac{(1+z)\ {}_2F_1\left(\frac{1}{3}, \frac{1}{2}; \frac{4}{3}; -\frac{\Omega_m}{\Omega_\Lambda}(1+z)^3\right) - {}_2F_1\left(\frac{1}{3}, \frac{1}{2}; \frac{4}{3}; -\frac{\Omega_m}{\Omega_\Lambda}\right)}{H_{\text{obs}} \sqrt{\Omega_\Lambda}} \tag{38}$$

The area of the photon sphere is then:

$$A_{\text{ph}}(z) = 4\pi a^2(t_{\text{obs}}) r^2(z) = 4\pi r^2(z) \tag{39}$$

The second sphere is the bursts sphere. It has its origin at the observer's position, and the radius the same as the photon sphere. Therefore, its area is:

$$A_{\text{b}}(z) = 4\pi a^2(0) r^2(z) = \frac{4\pi r^2(z)}{(1+z)^2} \tag{40}$$

We need to know one more thing about the bursts sphere – the volume of the infinitesimal shell surrounding it. For that we can again use the metric:

$$\begin{aligned}
\mathrm{d}V(z) &= -A_{\mathrm{b}}(z)\, a(0)\, \mathrm{d}r \\
&= -A_{\mathrm{b}}(z)\, a(0) \frac{\mathrm{d}a}{a^2(0)\, H_{\mathrm{obs}} \sqrt{\Omega_m \frac{1}{a^3(t)} + \Omega_\Lambda}} \\
&= A_{\mathrm{b}}(z) \frac{\frac{1}{(1+z)^2}\, \mathrm{d}z\, (1+z)}{H_{\mathrm{obs}} \sqrt{\Omega_m \frac{1}{a^3(t)} + \Omega_\Lambda}} \\
&= A_{\mathrm{b}}(z) \frac{1}{(1+z)} \frac{\mathrm{d}z}{H_{\mathrm{obs}} \sqrt{\Omega_m (1+z)^3 + \Omega_\Lambda}} \\
&= \frac{4\pi r^2(z)}{(1+z)^3} \frac{\mathrm{d}z}{H_{\mathrm{obs}} \sqrt{\Omega_m (1+z)^3 + \Omega_\Lambda}}
\end{aligned} \tag{41}$$

References

[1] G. Vianello, "Observations of Gamma-ray Bursts in the Fermi era," 2013.

[2] N. Gehrels and S. Razzaque, "Gamma Ray Bursts in the Swift-Fermi Era," *Front.Phys.China.*, vol. 8, pp. 661–678, 2013.

[3] J. S. Bloom, D. Frail, and S. Kulkarni, "GRB energetics and the GRB Hubble diagram: Promises and limitations," *Astrophys.J.*, vol. 594, pp. 674–683, 2003.

[4] T.-F. Yi, E.-W. Liang, Y.-P. Qin, and R.-J. Lu, "On the spectral lags of the short gamma-ray bursts," *Mon.Not.Roy.Astron.Soc.*, vol. 367, pp. 1751–1756, 2006.

[5] G. Castignani, D. Guetta, E. Pian, L. Amati, S. Puccetti, *et al.*, "Time delays between Fermi LAT and GBM light curves of GRBs," 2014.

[6] J. Lange and M. Pohl, "The average GeV-band Emission from Gamma-Ray Bursts," 2013.

[7] M. Ackermann *et al.*, "The Fermi Large Area Telescope On Orbit: Event Classification, Instrument Response Functions, and Calibration," *Astrophys.J.Suppl.*, vol. 203, p. 4, 2012.

[8] M. Ackermann, M. Ajello, K. Asano, M. Axelsson, L. Baldini, *et al.*, "The First Fermi-LAT Gamma-Ray Burst Catalog," *Astrophys.J.Suppl.*, vol. 209, p. 11, 2013.

[9] G. Rubtsov, M. Pshirkov, and P. Tinyakov, "GRB observations by Fermi LAT revisited: new candidates found," *Mon.Not.Roy.Astron.Soc.Lett.*, vol. 421, pp. L14–L18, 2012.

[10] H. Tajima, "Fermi Observations of high-energy gamma-ray emissions from GRB 080916C," 2009.

[11] M. Ackermann *et al.*, "Fermi Observations of GRB 090510: A Short Hard Gamma-Ray Burst with an Additional, Hard Power-Law Component from 10 keV to GeV Energies," *Astrophys.J.*, vol. 716, pp. 1178–1190, 2010.

[12] A. Abdo *et al.*, "Fermi Observations of GRB 090902B: A Distinct Spectral Component in the Prompt and Delayed Emission," *Astrophys.J.*, vol. 706, pp. L138–L144, 2009.

[13] M. Ackermann *et al.*, "Detection of a spectral break in the extra hard component of GRB 090926A," *Astrophys.J.*, vol. 729, p. 114, 2011.

[14] T. Nakamura and K. Ioka, "Peak luminosity-spectral lag relation caused by the viewing angle of the collimated gamma-ray bursts," 2001.

[15] R.-F. Shen, L.-M. Song, and Z. Li, "Spectral lags and the energy dependence of pulse width in gamma-ray bursts: Contributions from the relativistic curvature effect," *Mon.Not.Roy.Astron.Soc.*, vol. 362, pp. 59–65, 2005.

[16] A. Shenoy, E. Sonbas, C. Dermer, L. Maximon, K. Dhuga, *et al.*, "Probing Curvature Effects in the Fermi GRB 110920," *Astrophys.J.*, vol. 778, p. 3, 2013.

[17] G. Ghirlanda, L. Nava, G. Ghisellini, A. Celotti, D. Burlon, *et al.*, "Gamma Ray Bursts in the comoving frame," 2011.